arXiv:1411.6790v1 [cond-mat.mtrl-sci] 25 Nov 2014

Longitudinal spin Seebeck effect contribution in transverse spin Seebeck effect experiments in Pt/YIG and Pt/NFO

D. Meier,[1,*] D. Reinhardt,[1] M. van Straaten,[1] C. Klewe,[1] M. Althammer,[2] M. Schreier,[2,3] S.T.B. Goennenwein,[2,4] A. Gupta,[5] M. Schmid,[6] C.H. Back,[6] J.-M. Schmalhorst,[1] T. Kuschel,[1] and G. Reiss[1]

[1] *Department of Physics, Center for Spinelectronic Materials and Devices, Bielefeld University, 33501 Bielefeld, Germany*
[2] *Walther-Meissner-Institut, Bayerische Akademie der Wissenschaften, Walther-Meissner-Strasse 8, 85748 Garching, Germany*
[3] *Physik-Department, Technische Universität München, 85748 Garching, Germany*
[4] *Nanosystems Initiative Munich (NIM), Schellingstraße 4, 80799 München, Germany*
[5] *Center for Materials for Information Technology, University of Alabama, Tuscaloosa Alabama 35487, USA*
[6] *Institute of Experimental and Applied Physics, University of Regensburg, 93040, Germany*

(Dated: November 26, 2014)

We investigate the inverse spin Hall voltage of a 10 nm thin Pt strip deposited on the magnetic insulators $Y_3Fe_5O_{12}$ (YIG) and $NiFe_2O_4$ (NFO) with a temperature gradient in the film plane. We observe characteristics typical of the spin Seebeck effect, although we do not observe a change of sign of the voltage at the Pt strip when it is moved from hot to cold side, which is believed to be the most striking feature of the *transverse* spin Seebeck effect. Therefore, we relate the observed voltages to the *longitudinal* spin Seebeck effect generated by a parasitic out-of-plane temperature gradient, which can be simulated by contact tips of different material and heat conductivities and by tip heating. This work gives new insights into the interpretation of transverse spin Seebeck effect experiments, which are still under discussion.

Spin caloritronics is an active branch in spintronics [1, 2]. The interplay between heat, charge and spin transport opens a new area of fascinating issues involving the use of waste heat in electronic devices. One potentially useful effect for heat harvesting [3] is the spin Seebeck effect (SSE) [4] which was observed in 2008.

It was reported that a spin current perpendicular to an applied temperature gradient can be generated in a ferromagnetic metal (FMM) by the transverse spin Seebeck effect (TSSE) [4]. An adjacent normal metal (NM) converts the spin current via the inverse spin Hall effect (ISHE) [5] into a transverse voltage, which is antisymmetric with respect to the external magnetic field H ($V(H) = -V(-H)$, cf. Fig. 1 (a)). In this geometry, the temperature gradient is typically aligned in-plane (∇T_x) and can also induce a planar Nernst effect (PNE) in FMM with magnetic anisotropy [6] which is due to the anisotropic magnetic thermopower and symmetric with respect to H ($V(H) = V(-H)$). For pure ∇T_x in a ferro(i)magnetic insulator (FMI) there is no PNE, since there are no free charge carriers available. However, if the NM material is close to the Stoner criterion, a static magnetic proximity effect could induce a so called proximity PNE, which in general is present in spin polarized NM adjacent to a FMM and could also occur in a NM-FMI contact (cf. Fig. 1 (a)).

For the longitudinal SSE (LSSE) [7] the spin current flows directly from the FM into an adjacent NM parallel to the temperature gradient (cf. Fig. 1 (b)), which is typically aligned out-of-plane (∇T_z). In NM/FMM bilayers the anomalous Nernst effect (ANE) can occur, but is absent in the FMI. In semiconducting materials the ANE contributes to the LSSE as already shown for Pt/NFO at room temperature [8]. Additionally, if the NM would be spin polarized by the proximity to the FM, an additional proximity ANE could occur [9] (cf. Fig. 1 (b)).

We would like to point out that Figs. 1 (a) and 1 (b) include results of previous experiments with pure ∇T_x on NM/FMM [4, 6, 10, 11] and on NM/FMI [7] as well as

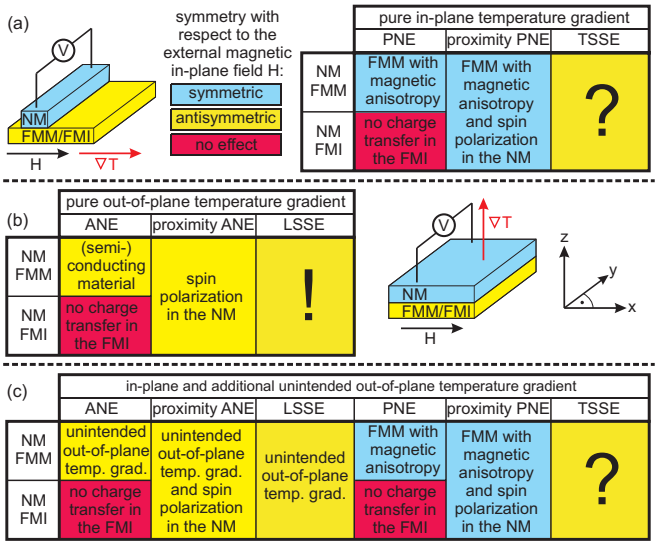

FIG. 1. Summary of effects in SSE experiments for NM/FMM and NM/FMI bilayers and given symmetry with respect to the external magnetic in-plane field H for antisymmetric magnetization reversal processes. (a) Pure in-plane ∇T for TSSE measurements. (b) Pure out-of-plane ∇T for LSSE measurements. (c) In-plane and unintended out-of-plane ∇T.

pure ∇T_z on NM/FMM [8] and on NM/FMI [12–19]. As summarized in Fig. 1 (c) an unintended ∇T_z can hamper the evaluation of TSSE experiments with applied ∇T_x. Heat flow into the surrounding area or through the electrical contacts can induce an additional ANE in NM/FMM bilayers and NM/magnetic semiconductors as discussed in literature [11, 20–24]. But since, in principle, all the effects of an LSSE experiment can be present in the TSSE experiment with unintended ∇T_z, proximity Nernst effects and especially parasitic LSSE can also be present in NM/FMI bilayers as already mentioned recently [25]. This leads to four possible effects which are antisymmetric with respect to the external magnetic field, when the temperature gradient is not controlled very carefully (cf. Fig. 1 (c)). These phenomena and discussions of side-effects in TSSE experiments have not been treated systematically in the literature up to now for NM/FMI bilayers and will be investigated in this study.

The YIG films in our experiments had a thickness of $t_{\mathrm{YIG}} = 180\,\mathrm{nm}$ and were deposited on gadolinium gallium garnet ($Gd_3Ga_5O_{12}$, GGG) (111)-oriented single crystal substrates with width and length $w = l = 5\,\mathrm{mm}$ by pulsed laser deposition (PLD) from a stoichiometric polycrystalline target. The films show a coercive field of about 100 Oe and a saturation magnetization of $M_S = 120\,\mathrm{kA/m}$. The NFO films with a thickness of about $t_{\mathrm{NFO}} = 1\,\mu\mathrm{m}$ were deposited on $10 \times 5\,\mathrm{mm}^2$ $MgAl_2O_4$ (MAO) (100)-oriented substrates by direct liquid injection chemical vapor deposition (DLI-CVD)[8, 26]. After a vacuum break and cleaning with ethanol in an ultrasonic bath a $t_{\mathrm{Pt}} = 10\,\mathrm{nm}$ thin Pt strip was deposited by dc magnetron sputtering in an Ar atmosphere of $1.5 \times 10^{-3}\,\mathrm{mbar}$ through a 100 µm wide split-mask on one sample side of the YIG and NFO films with a length of $l_{\mathrm{Pt}} = 5\,\mathrm{mm}$.

For the experiments we used the same setup and technique described in Ref. [11]. The experiments are conducted under ambient conditions and the ends of the Pt strip were contacted with a microprobe system with Au and W tips of different diameters. Furthermore, one set of Au tips was equipped with a $1.5\,\mathrm{k\Omega}$ resistor for heating the tip to intentionally induce a ∇T_z (cf. Fig. 2 (a)) [11]. Fig. 2 (b) shows the nearly linear relation between the power P_{needle} dissipated in the resistor and the tip temperature T_{needle} as determined with a type-K thermocouple glued to the tip in a calibration measurement. The voltage V at the Pt strip was measured with a Keithley 2182A nanovoltmeter. An external magnetic field H was applied along x in a range of ±600 Oe for YIG and of ±1000 Oe for NFO films.

First, the ISHE voltage from the Pt/YIG sample was measured for various ΔT_x. The Pt strip was on the hot side and contacted with W tips. The voltage shows no significant variation within the sensitivity limit when H is varied (Fig. 3 (a)). No Nernst effects are observed due to the insulating magnetic layer and no evidence for an additional ∇T_z can be detected. Therefore, the clamping and heating of the sample in our setup and the contacting with thin W tips results in a pure ∇T_x as already shown in Ref. [11]. TSSE is not observable although the Pt strip is located near the hot side of the YIG film and far away from the center where the TSSE should vanish.

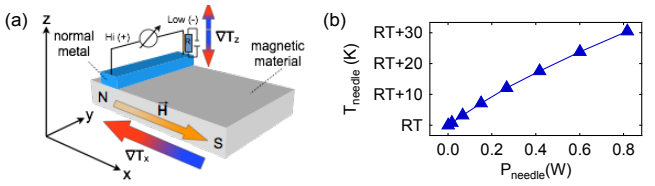

FIG. 2. (a) Measurement configuration: In-plane temperature gradient ∇T_x applied parallel to the external magnetic field $\vec{H}$ in the x-direction. An additional out-of-plane temperature gradient ∇T_z can be induced by using thick contact tips or heating one tip with a voltage on a resistor R attached to the tip. (b) the temperature T_{needle} at the tip of the Au needle as a function of the power P_{needle} at the resistor R (only thermally connected to the contact needle, not electrically).

In the next step we created a second heat sink by using thicker Au tips (Fig. 3 (b)). The diameter of the contact area is of about 500 µm in contrast to the contact area with W tips of about 10 µm. It can be seen that the measured voltage now shows an antisymmetric behavior with respect to magnetic field inversion (Fig. 3 (b)-(e)). Next, we applied a voltage to the Au tip resistor to heat the needle and change the out-of-plane heat flow. The heated Au needle is labeled $T_{\mathrm{needle}} = \mathrm{RT} + \mathrm{x}$ with room temperature $\mathrm{RT} = 296\,\mathrm{K}$. The magnitude V_{sat} (the voltage in saturation) is calculated with $(V_+ - V_-)/2$ for the average voltage $V_\pm$ in the region of $500\,\mathrm{Oe} < H < 600\,\mathrm{Oe}$ and $-600\,\mathrm{Oe} < H < -500\,\mathrm{Oe}$ for Pt/YIG as well as $900\,\mathrm{Oe} < H < 1000\,\mathrm{Oe}$ and $-1000\,\mathrm{Oe} < H < -900\,\mathrm{Oe}$ for Pt/NFO, respectively.

In Fig. 3 (b) for $T_{\mathrm{needle}} = \mathrm{RT}$ a small antisymmetric effect of about $V_{\mathrm{sat}} = -50\,\mathrm{nV}$ is obtained when the Pt strip is at the cold side of the YIG film. When the needle is heated to $T_{\mathrm{needle}} = \mathrm{RT} + 12\,\mathrm{K}$ the ISHE voltage changes its sign to a value of $V_{\mathrm{sat}} = +95\,\mathrm{nV}$ and changes further to $V_{\mathrm{sat}} = +590\,\mathrm{nV}$ for $T_{\mathrm{needle}} = \mathrm{RT} + 24\,\mathrm{K}$. By using these Au needles with large contact areas an additional small out-of-plane heat flow is generated even at the cold side of the sample. This heat flow changes its sign with increasing T_{needle} which can be detected by the sign reversal of the measured voltage. When ∇T_x is increased ($\Delta T_x = 30\,\mathrm{K}$ in Fig. 3 (c)) the ISHE voltage at the Pt is $V_{\mathrm{sat}} = -170\,\mathrm{nV}$ for $T_{\mathrm{needle}} = \mathrm{RT}$ and therefore three times larger than for $\Delta T_x = 10\,\mathrm{K}$. The ISHE voltage again increases with increasing T_{needle} and changes sign.

For a Pt strip at the hot side V_{sat} without tip heating is larger than at the cold side. For $\Delta T_x = 5\,\mathrm{K}$ the magnitude is about $V_{\mathrm{sat}} = -130\,\mathrm{nV}$ (Fig. 3 (d)) which can be

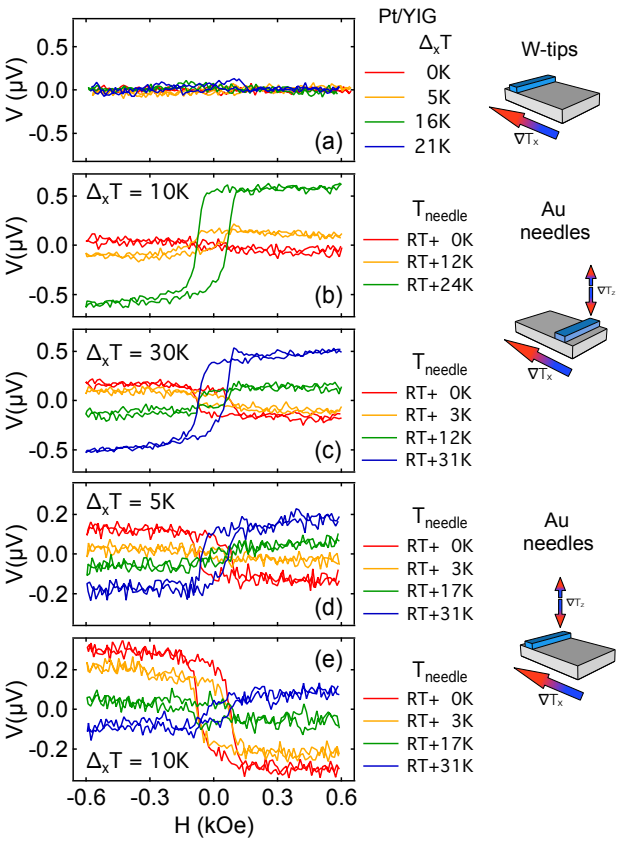

FIG. 3. (a) H dependence of V measured at the Pt strip on YIG located (a) at the hot side using thin W tips without inducing an additional ∇T_z for various ∇T_x, (b)-(e) using thick Au tips and different tip heating voltages (b) at the cold side for $\Delta T_x = 10\,\mathrm{K}$, (c) at the cold side for $\Delta T_x = 30\,\mathrm{K}$, (d) at the hot side for $\Delta T_x = 5\,\mathrm{K}$ and (e) at the hot side for $\Delta T_x = 10\,\mathrm{K}$.

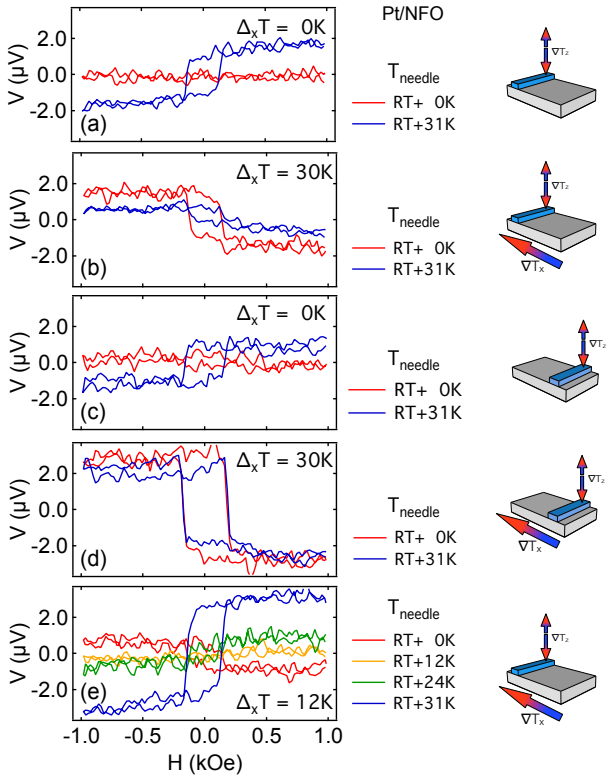

FIG. 4. (a)-(d) V as a function of H measured at a Pt strip on NFO using thick Au needles (a) at the hot side for $\Delta T_x = 0\,\mathrm{K}$, (b) at the hot side for $\Delta T_x = 30\,\mathrm{K}$, (c) at the cold side for $\Delta T_x = 0\,\mathrm{K}$, (d) at the cold side for $\Delta T_x = 30\,\mathrm{K}$, and (e) at the hot side with $\Delta T_x = 12\,\mathrm{K}$ and different Au tip heating voltages.

decreased to $V_{\mathrm{sat}} = -300\,\mathrm{nV}$ for $\Delta T_x = 10\,\mathrm{K}$ (Fig. 3 (e)). The sign and the magnitude of V_{sat} can also be controlled by T_{needle} and, therefore, by ∇T_z. When T_{needle} is fixed at $\mathrm{RT} + 31\,\mathrm{K}$, V_{sat} is about $+180\,\mathrm{nV}$ for $\Delta T_x = 5\,\mathrm{K}$ and $+90\,\mathrm{nV}$ for $\Delta T_x = 10\,\mathrm{K}$.

For a verification of this behavior in another material system, NFO films with a Pt strip were used and contacted with Au needles. When $\Delta T_x = 0\,\mathrm{K}$ and no tip heating is applied no significant change in V as a function of H is observed (Fig. 4 (a)). This behavior is the same for Pt strips on both sides of the NFO film (Fig. 4 (c)).

When a ∇T_x is applied, the same sign of V_{sat} on both sides is achieved (Fig. 4 (b),(d)). The effect can again be manipulated by applying a needle temperature of $T_{\mathrm{needle}} = \mathrm{RT} + 31\,\mathrm{K}$. The discrepancy for Pt/NFO measurements on hot side (smaller $|V_{\mathrm{sat}}|$, Fig. 4 (b)) and cold side (larger $|V_{\mathrm{sat}}|$, Fig. 4 (d)) compared to Pt/YIG on hot side (larger $|V_{\mathrm{sat}}|$, Fig. 3 (e)) and cold side (smaller $|V_{\mathrm{sat}}|$, Fig. 3 (b)) can be explained by contacting the needles again after reversing the sample to "move" the Pt strip from the hot to the cold side. The real contact area between the tips and the Pt can be different when the sample is remounted. Furthermore, T_{needle} was varied for $\Delta T_x = 12\,\mathrm{K}$ (Fig. 4 (e)). V_{sat} at $T_{\mathrm{needle}} = \mathrm{RT}$ is about $+690\,\mathrm{nV}$. The absolute value is more than two times smaller than for $\Delta T_x = 30\,\mathrm{K}$ ($V_{\mathrm{sat}} = -1550\,\mathrm{nV}$) with the change of ΔT_x. V_{sat} also vanishes for $T_{\mathrm{needle}} = \mathrm{RT} + 12\,\mathrm{K}$ and changes sign for increasing T_{needle}.

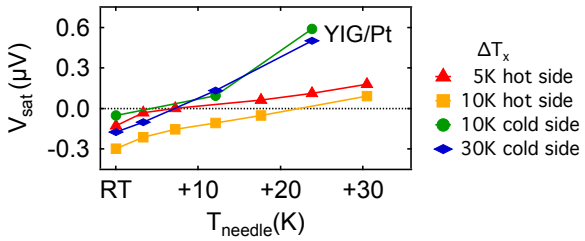

FIG. 5. V_{sat} as a function of the Au needle temperature T_{needle} for various in-plane temperature differences ΔT_x in Pt/YIG.

V_{sat} measured for Pt/YIG at the hot and cold side is plotted as a function of T_{needle} for different ΔT_{x} in Fig. 5. A non-heated Au needle results in the same sign of V_{sat} for all ΔT_{x}, while $|V_{\mathrm{sat}}|$ is smaller on the cold side compared to the hot side. We explain this behaviour of V_{sat} by an unintended heat flux through the Au needles leading to a vertical temperature gradient ∇T_{z} and, therefore, to a LSSE induced spin current into the Pt. We point out, that the sign of the resulting voltage at the Pt strip is quantitatively consistent with the magnitude of the recent LSSE reported by Schreier et al. [27] from comparative experiments performed in different groups if we consider an unintended out-of-plane ∇T_{z} pointing into -z direction. For a heated Au needle V_{sat} increases and crosses zero (cf. Fig. 5). Here, the tip heating compensates the out-of-plane heat flux induced by ΔT_{x} ($\nabla T_{\mathrm{z}} = 0$). After the sign change of V_{sat} (and therefore, ∇T_{z}), the values increases with a larger (smaller) slope for the cold (hot) side.

Xiao et al. [28] discussed the temperature difference ΔT_{me} between the magnon temperature in the FM and the electron temperature in the NM as the origin of the thermally induced spin current. ΔT_{me} can be inferred from the recorded voltage as [25, 28]

$$\Delta T_{\mathrm{me}} = \frac{V_{\mathrm{sat}}\,\pi\,M_{\mathrm{S}}\,V_{\mathrm{a}}\,t_{\mathrm{Pt}}}{g_{\mathrm{r}}\,\gamma\,k_{\mathrm{B}}\,e\,\Theta_{\mathrm{SH}}\,\rho_{\mathrm{Pt}}\,l_{\mathrm{Pt}}\,\lambda\,\tanh(t/2\lambda)}. \qquad (1)$$

Here, V_{a} is the magnetic coherence volume, g_{r} is the real part of the spin mixing conductance, γ is the gyromagnetic ratio, k_{B} is the Boltzmann constant, e is the elementary charge, Θ_{SH} is the spin Hall angle, and λ is the spin diffusion length of the NM material. The two temperature model has proven successful in relating ΔT_{me} to the phonon temperature, accessible in experiments [25, 29]. We simulate the phonon and magnon temperatures assuming 1D transport in our films and disregard the influence of thermal contact resistance other than the coupling between magnons and electrons. This yields a value ΔT_{z}, the (phonon) temperature drop across the YIG film, for which the experimentally measured V_{sat} is obtained. We assume $\rho_{\mathrm{Pt}} = 40\,\mu\Omega\,\mathrm{cm}$. All material dependent YIG parameters were taken from Ref. [25].

We calculated ΔT_{me} for the largest and smallest V_{sat} taken from Fig. 5 at RT (red curves in Fig. 3 (b) and (e)) and the corresponding ΔT_{z}. For $|V_{\mathrm{sat}}| = 50\,\mathrm{nV}$ (cf. Fig. 3 (b)) we obtain $\Delta T_{\mathrm{me}} = 0.5\,\mu\mathrm{K}$ and a corresponding $\Delta T_{\mathrm{z}} = 2\,\mathrm{mK}$. For $|V_{\mathrm{sat}}| = 300\,\mathrm{nV}$ (cf. Fig. 3 (e)) the corresponding values are $\Delta T_{\mathrm{me}} = 3.2\,\mu\mathrm{K}$ and $\Delta T_{\mathrm{z}} = 12\,\mathrm{mK}$. The obtained ΔT_{z} are in the order of a few millikelvins. It is reasonable to assume that such values can be induced by e.g. thick contact tips, especially considering that our initial simplifications should lead to an overestimation of ΔT_{z} [25]. The transverse spin Seebeck configuration was investigated in detail in Ref. [25]. It was found that for $\Delta T_{\mathrm{x}} = 20\,\mathrm{K}$ the obtained ΔT_{me} is well below 1 µK, even at the very edge of the sample where ΔT_{me} is maximized. This further supports the notion that spurious out-of-plane gradients are responsible for the voltages observed in our samples.

The different magnitudes in voltage for Pt/NFO compared to Pt/YIG can be explained by different contact areas of the tips, different thicknesses and thermal conductivities between NFO and YIG as well as different spin mixing conductances [30, 31]. However, for both sample systems the spin mixing conductance should be large enough to observe a thermally driven spin current across the NM/FMI interface, since we clearly observe an LSSE due to the Au tip heating induced ΔT_{z}.

In addition to the LSSE, we now discuss other parasitic effects like the ANE and proximity ANE, which can be produced by an unintended ΔT_{z} (see Fig. 1). We can exclude an ANE for YIG due to the lack of charge carriers. For NFO we observed an ANE which is one order of magnitude smaller at RT than the LSSE [8]. This ANE can be explained by the weak conductance of NFO at RT due to thermal activation energies of a few hundred meV depending on the preparation technique [8, 32]. The proximity ANE in Pt/NFO can also be excluded, since no spin polarization was found using x-ray resonant magnetic reflectivity (XRMR) measurements, which are very sensitive to the interface spin polarization [33]. In case of Pt/YIG Geprägs et al. presented x-ray magnetic circular dichroism measurements (XMCD) with no evidence for any spin polarization in Pt [34], while Lu et al. could show XMCD measurements indicating magnetic moments in Pt on their YIG samples [35]. Future investigations with XRMR can give more insight to this discrepancy. However, Kikkawa et al. could show that a potential contribution of a proximity ANE additional to the LSSE is negligibly small [36]. This supports our conclusion, that the main antisymmetric contribution in our measurements on both Pt/YIG and Pt/NFO is the LSSE, which is driven by an out-of-plane temperature gradient.

We do not observe any symmetric contribution for ∇T_{x} without tip heating. Therefore, PNE and proximity PNE contributions can also be excluded. Nevertheless, we find a small symmetric contribution for strong tip heating as demonstrated in Fig. 3 (c) for $\Delta T_{\mathrm{needle}} = \mathrm{RT} + 31\,\mathrm{K}$. In the region of H_C small peaks are visible under symmetrization of the voltage. This hints at the existence of an additional magnetothermopower effect potentially induced by a temperature gradient ∇T_{y} and will be part of future investigations.

Recently, Wegrowe et al. [37] used anisotropic heat-transport as an interpretation for the measured voltages using in-plane temperature gradients. In their work, they derived the anisotropic field-dependent temperature gradient in FMM and FMI from the Onsager reciprocity relations. Therefore, the thermocouple effect between the FM, the NM and the contacting tips can generate field-

dependent voltages if there is a difference in the Seebeck coefficients. In our investigated systems, the Seebeck coefficients are indeed different for FM, Pt and the contact tips. However, since we do not observe a field-dependent variation of the ISHE voltage by using W tips, any anisotropic field-dependent heat-transport can be excluded as the reason for the observed voltages.

In summary, we investigated the relevance of TSSE in Pt/YIG and Pt/NFO systems. We found no significant ISHE voltages upon applying an in-plane temperature gradient and using sharp W tips (10 µm contact diameter) for the electrical contacting. However, upon using tips with more than 100 µm diameter contact area, which induce an additional out-of-plane temperature gradient, an antisymmetric contribution to the ISHE voltage of the Pt strip could be introduced at will. This antisymmetric effect can be identified as LSSE which was verified by controlling the needle temperature and varying the out-of-plane temperature gradient. Taken together, in all our experiments, we thus only observe LSSE-type signatures. These LSSE voltages can be reminiscent of a TSSE-type response if an unintentional (or intentional) ∇T_z is present. This shows that utmost care is required if one is to interpret magnetothermopower effects in terms of the TSSE.

We thank the DFG (SPP 1538) and the EMRP JRP EXL04 SpinCal for financial support. The EMRP is jointly funded by the EMRP participating countries within EURAMET and the EU.

* dmeier@physik.uni-bielefeld.de; www.spinelectronics.de

[1] G. E. W. Bauer, E. Saitoh, and B. J. van Wees, Nature Materials **11**, 391 (2012).
[2] S. A. Wolf, D. D. Awschalom, R. A. Buhrman, J. M. Daughton, S. von Molnár, M. L. Roukes, A. Y. Chtchelkanova, and D. M. Treger, Science **294**, 1488 (2001).
[3] A. Kirihara, K. Uchida, Y. Kajiwara, M. Ishida, Y. Nakamura, T. Manako, E. Saitoh, and S. Yorozu, Nature Materials **11**, 686 (2012).
[4] K. Uchida, S. Takahashi, K. Harii, J. Ieda, W. Koshibae, K. Ando, S. Maekawa, and E. Saitoh, Nature **455**, 778 (2008).
[5] E. Saitoh, M. Ueda, H. Miyajima, and G. Tatara, Applied Physics Letters **88**, 182509 (2006).
[6] A. Avery, M. Pufall, and B. Zink, Physical Review Letters **109**, 196602 (2012).
[7] K. Uchida, H. Adachi, T. Ota, H. Nakayama, S. Maekawa, and E. Saitoh, Applied Physics Letters **97**, 172505 (2010).
[8] D. Meier, T. Kuschel, L. Shen, A. Gupta, T. Kikkawa, K. Uchida, E. Saitoh, J. M. Schmalhorst, and G. Reiss, Physical Review B **87**, 054421 (2013).
[9] G. Y. Guo, Q. Niu, and N. Nagaosa, Physical Review B **89**, 214406 (2014).
[10] C. M. Jaworski, J. Yang, S. Mack, D. D. Awschalom, J. P. Heremans, and R. C. Myers, Nature Materials **9**, 898 (2010).
[11] D. Meier, D. Reinhardt, M. Schmid, C. H. Back, J. M. Schmalhorst, T. Kuschel, and G. Reiss, Physical Review B **88**, 184425 (2013).
[12] K. Uchida, H. Adachi, T. Ota, H. Nakayama, S. Maekawa, and E. Saitoh, Applied Physics Letters **97**, 172505 (2010).
[13] K. Uchida, T. Nonaka, T. Ota, and E. Saitoh, Applied Physics Letters **97**, 262504 (2010).
[14] S. Y. Huang, X. Fan, D. Qu, Y. P. Chen, W. G. Wang, J. Wu, T. Y. Chen, J. Q. Xiao, and C. L. Chien, Physical Review Letters **109**, 107204 (2012).
[15] M. Weiler, M. Althammer, F. Czeschka, H. Huebl, M. Wagner, M. Opel, I.-M. Imort, G. Reiss, A. Thomas, R. Gross, and S. Goennenwein, Physical Review Letters **108**, 106602 (2012).
[16] D. Qu, S. Y. Huang, J. Hu, R. Wu, and C. L. Chien, Physical Review Letters **110**, 067206 (2013).
[17] A. Kehlberger, G. Jakob, M. C. Onbasli, D. H Kim, C. A. Ross, and M. Kläui, Journal of Applied Physics **115**, 17C731 (2014).
[18] G. Siegel, M. C. Prestgard, S. Teng, and A. Tiwari, Scientific Reports **4** (2014).
[19] M. Agrawal, V. I. Vasyuchka, A. A. Serga, A. Kirihara, P. Pirro, T. Langner, M. B. Jungfleisch, A. V. Chumak, E. T. Papaioannou, and B. Hillebrands, Physical Review B **89**, 224414 (2014).
[20] S. Bosu, Y. Sakuraba, K. Uchida, K. Saito, T. Ota, E. Saitoh, and K. Takanashi, Physical Review B **83** (2011).
[21] S. Huang, W. Wang, S. Lee, J. Kwo, and C. Chien, Physical Review Letters **107**, 196602 (2011).
[22] M. Schmid, S. Srichandan, D. Meier, T. Kuschel, J. M. Schmalhorst, M. Vogel, G. Reiss, C. Strunk, and C. H. Back, Physical Review Letters **111**, 187201 (2013).
[23] C. T. Bui and F. Rivadulla, Phys. Rev. B **90**, 100403 (2014).
[24] I. V. Soldatov, N. Panarina, C. Hess, L. Schultz, and R. Schäfer, Phys. Rev. B **90**, 104423 (2014).
[25] M. Schreier, A. Kamra, M. Weiler, J. Xiao, G. E. W. Bauer, R. Gross, and S. T. B. Goennenwein, Phys. Rev. B **88**, 094410 (2013).
[26] N. Li, Y.-H. A. Wang, M. N. Iliev, T. M. Klein, and A. Gupta, Chemical Vapor Deposition **17**, 261 (2011).
[27] M. Schreier, G. E. W. Bauer, V. Vasyuchka, J. Flipse, K. Uchida, J. Lotze, V. Lauer, A. Chumak, A. Serga, S. Daimon, T. Kikkawa, E. Saitoh, B. J. van Wees, B. Hillebrands, R. Gross, and S. T. B. Goennenwein, arXiv:1404.3490 (2014).
[28] J. Xiao, G. Bauer, K. Uchida, E. Saitoh, and S. Maekawa, Physical Review B **81** (2010).
[29] J. Flipse, F. L. Bakker, A. Slachter, F. K. Dejene, and B. J. van Wees, Nature Nanotechnology **7**, 166 (2012).
[30] M. Weiler, M. Althammer, M. Schreier, J. Lotze, M. Pernpeintner, S. Meyer, H. Huebl, R. Gross, A. Kamra, J. Xiao, Y.-T. Chen, H. Jiao, G. E. W. Bauer, and S. T. B. Goennenwein, Physical Review Letters **111**, 176601 (2013).
[31] Z. Qiu, K. Ando, K. Uchida, Y. Kajiwara, R. Takahashi, H. Nakayama, T. An, Y. Fujikawa, and E. Saitoh, Applied Physics Letters **103**, 092404 (2013).
[32] C. Klewe, M. Meinert, A. Boehnke, K. Kuepper, E. Arenholz, A. Gupta, J. M. Schmalhorst, T. Kuschel, and

G. Reiss, Journal of Applied Physics **115**, 123903 (2014).
[33] T. Kuschel, C. Klewe, J. M. Schmalhorst, F. Bertram, O. Schuckmann, T. Schemme, J. Wollschläger, S. Francoual, J. Strempfer, A. Gupta, M. Meinert, G. Götz, D. Meier, and G. Reiss, arXiv:1411.0113 (2014).
[34] S. Geprägs, S. Meyer, S. Altmannshofer, M. Opel, F. Wilhelm, A. Rogalev, R. Gross, and S. T. B. Goennenwein, Applied Physics Letters **101**, 262407 (2012).
[35] Y. Lu, Y. Choi, C. Ortega, X. Cheng, J. Cai, S. Huang, L. Sun, and C. Chien, Physical Review Letters **110**, 147207 (2013).
[36] T. Kikkawa, K. Uchida, Y. Shiomi, Z. Qiu, D. Hou, D. Tian, H. Nakayama, X. F. Jin, and E. Saitoh, Physical Review Letters **110**, 067207 (2013).
[37] J. E. Wegrowe, H. J. Drouhin, and D. Lacour, Physical Review B **89**, 094409 (2014).